Fluid Antenna-Assisted ISAC Systems

Liaoshi Zhou, Junteng Yao, Ming Jin, Tuo Wu, and Kai-Kit Wong, *Fellow*, *IEEE*

Abstract—This letter proposes a fluid antenna-assisted integrated sensing and communication (ISAC) system, where a base station (BS) transmits signals to a communication user (CU) while sensing a target. Unlike traditional ISAC systems with fixed-position antennas (FPAs), fluid antennas are equipped at the BS and CU, and can be dynamically adjusted within a given area. Our objective is to jointly optimize the transmit beamforming and the locations of fluid antennas at the BS and CU to maximize the downlink communication rate while ensuring the requirements of the sensing beampattern gain and transmit power of the BS. Due to the non-convex nature of the original problem and the high coupling between variables, we employ an alternating optimization (AO) algorithm, dividing it into three subproblems and transforming them into convex ones for solution. Simulation results confirm that our proposed system significantly improves the performance of ISAC systems compared to benchmarks.

Index Terms—Fluid antenna, integrated sensing and communication (ISAC), alternating optimization (AO).

I. Introduction

W ITH the advent of the sixth generation (6G) of wireless networks, massive connectivity has become an inevitable trend for future networks [1]. However, spectrum scarcity remains a critical challenge for the development of these networks. To overcome this challenge, integrated sensing and communication (ISAC) has been identified as a promising solution that can simultaneously support wireless communication and sensing using the radar spectrum resource [2], [3], [4]. Recently, ISAC has attracted considerable interest due to its high spectral efficiency. Consequently, it has been deployed in various wireless systems, including ISAC-assisted mobile edge computing (MEC) systems [5], ISAC-assisted wireless power transfer (WPT) systems [6], ISAC-assisted non-orthogonal multiple access (NOMA) systems [7], and ISAC-assisted physical layer security (PLS) systems [8].

To enhance the communication and sensing performance of ISAC systems, the incorporation of multiple-input multiple-output (MIMO) techniques has been proposed as an effective approach. Nevertheless, traditional MIMO systems with fixed-position antennas (FPAs) are unable to fully exploit spatial resources due to the immobility of antennas. To maximize the spatial degrees of freedom (DoFs) and further enhance ISAC performance, fluid antennas, a.k.a. movable antennas, can be utilized to overcome the limitations of FPAs [9], [10], [11], [12], [13]. The core concept of fluid antennas is that the antenna locations can be optimized within a certain region

L. Zhou, J. Yao, and M. Jin are with the faculty of Electrical Engineering and Computer Science, Ningbo University, Ningbo 315211, China (e-mail: {2311100202, yaojunteng, jinming}@nbu.edu.cn).

T. Wu is with the School of Electronic Engineering and Computer Science at Queen Mary University of London, London E1 4NS, U.K. (e-mail: tuo.wu@qmul.ac.uk).

K.-K. Wong is with the Department of Electronic and Electrical Engineering, University College London, WC1E 6BT London, U.K., and also with the Yonsei Frontier Laboratory and the School of Integrated Technology, Yonsei University, Seoul 03722, South Korea (e-mail: kai-kit.wong@ucl.ac.uk).

by controllers, thereby providing additional spatial DoFs [14]. Owing to the benefits of fluid antennas, their application has been extensively explored in various scenarios, including NOMA systems [15], secure communication systems [16], and over-the-air computation (AirComp) networks [17].

Inspired by these advancements, introducing fluid antennas into ISAC systems is the way forward. The primary advantage of this integration is the capability to optimize communication performance by dynamically adjusting the locations of fluid antennas. In traditional ISAC systems equipped with FPAs, the main path typically aligns with the target for sensing purposes, which can significantly impair communication performance. By strategically designing the locations of fluid antennas at both the transmitter and receiver, it is possible not only to maintain alignment with the sensing target but also to enhance communication performance. To the best of our knowledge, fluid antenna-assisted ISAC systems remain unexplored.

To address this research gap, this letter proposes a fluid antenna-assisted ISAC system. In our proposed system, a base station (BS) equipped with multiple fluid antennas transmits signals to a communication user (CU) equipped with a single fluid antenna and a sensing target equipped with a single FPA. Our aim is to maximize the communication rate under the sensing beampattern gain and transmit power of the BS constraints by jointly designing the transmit beamforming of the BS, the locations of transmit fluid antennas of the BS, and the location of a single receive fluid antenna of the CU. We employ the alternating optimization (AO) algorithm to tackle this highly non-convex problem. Simulation results indicate that the proposed scheme significantly outperforms benchmark approaches in terms of ISAC performance.

Notations: We use $\text{Tr}(\mathbf{A})$, $\mathbf{A}^H$, and $\mathbf{A}^T$ to denote the spectral norm, trace, conjugate transpose, and transpose, respectively; $\|\mathbf{a}\|_2$ denotes the 2-norm of vector $\mathbf{a}$; $\mathbf{A} \succeq \mathbf{0}$ indicates that $\mathbf{A}$ is positive semidefinite; $\Re\{x\}$ means the real part of x; $\mathcal{CN}(0, \sigma^2)$ denotes the distribution of a circularly symmetric complex Gaussian vector with mean 0 and covariance σ^2.

II. System Model and Problem Formulation

A. System Model

Consider an ISAC system comprising a dual-functional BS, a CU, and a sensing target. The BS simultaneously communicates with the CU and performs radar sensing directed towards a potential target. Both the BS and the CU are equipped with fluid antennas; the BS has $N(N \geq 2)$ fluid antennas while the CU is equipped with a single fluid antenna. These fluid antennas are connected to radio frequency (RF) chains via integrated waveguides or flexible cables, allowing free switching (or movement) within defined ranges, denoted as $\mathcal{S}_t$ for the BS and $\mathcal{S}_r$ for the CU, respectively. The location of the n-th fluid antenna of the BS is defined using a two-dimensional Cartesian coordinate model and can be

expressed as $\mathbf{t}_n = [x_n^t, y_n^t]^T, n \in \mathcal{N} = \{1, \ldots, N\}$. The collective locations of the BS's fluid antennas are represented as $\overline{\mathbf{t}} = [\mathbf{t}_1, \mathbf{t}_2, \ldots, \mathbf{t}_N] \in \mathbb{R}^{2 \times N}$. Similarly, the location of the CU's single fluid antenna is denoted by $\mathbf{r} = [x^r, y^r]^T$.

We define the beamforming vector of the BS as $\mathbf{v} \in \mathbb{C}^{N \times 1}$, and denote x as the transmit signal, used for both communication and radar sensing, with $\mathbb{E}[|x|^2] = 1$. Consequently, the received signal at the CU can be expressed as

$$\mathbf{y}(\overline{\mathbf{t}}, \mathbf{r}) = \mathbf{h}(\overline{\mathbf{t}}, \mathbf{r})\mathbf{v}x + w, \tag{1}$$

where $\mathbf{h}(\overline{\mathbf{t}}, \mathbf{r}) \in \mathbb{C}^{1 \times N}$ represents the channel vector from the BS to the CU, and $w \sim \mathcal{CN}(0, \sigma_w^2)$ denotes the additive white Gaussian noise at the CU.

B. Channel Model

We assume that the size of the 'moving'[1] region for the fluid antennas is significantly smaller than the distance between the transmitter and the receiver, thereby adopting the far-field model in this letter [11], [12]. Despite the mobility of the fluid antennas, the angles of arrival (AoA) and angles of departure (AoD) remain constant for each propagation path. The variation in signal propagation distance for the n-th antenna at the BS relative to its origin point $\mathbf{t}_0$ on the i-th transmit path is expressed as [18]

$$\rho_t^i(\mathbf{t}_n) = x_n^t \sin \phi_t^i \cos \psi_t^i + y_n^t \cos \phi_t^i, \tag{2}$$

where $\phi_t^i \in [0, \pi]$ and $\psi_t^i \in [0, \pi]$ represent the elevation and azimuth AoDs of the i-th path ($i \in \{1, \ldots, p_t\}$), respectively. Also, p_t denotes the number of transmit paths. Furthermore, the phase difference in the signal caused by the displacement of the n-th transmit fluid antenna from the origin point $\mathbf{t}_0$ on the i-th path is $\frac{2\pi}{\lambda} \rho_t^i(\mathbf{t}_n)$, where λ is the wavelength. This leads to the definition of the transmit response vector as

$$\mathbf{e}(\mathbf{t}_n) \triangleq \left[e^{j\frac{2\pi}{\lambda}\rho_t^1(\mathbf{t}_n)}, \ldots, e^{j\frac{2\pi}{\lambda}\rho_t^{p_t}(\mathbf{t}_n)} \right]^T \in \mathbb{C}^{p_t \times 1}, n \in \mathcal{N}. \tag{3}$$

Building upon (3), the far-field response matrix of the BS can be expressed as

$$\mathbf{E}(\overline{\mathbf{t}}) \triangleq [\mathbf{e}(\mathbf{t}_1), \mathbf{e}(\mathbf{t}_2), \ldots, \mathbf{e}(\mathbf{t}_N)]^T \in \mathbb{C}^{p_t \times N}. \tag{4}$$

Similarly, in the k-th receive path, the difference in propagation distance between the single receive fluid antenna at the CU and its reference point $\mathbf{r}_0$ is calculated as

$$\rho_r^k(\mathbf{r}) = x_n^r \sin \phi_r^k \cos \psi_r^k + y_n^r \cos \phi_r^k, \ k \in \{1, \ldots, p_r\}, \tag{5}$$

where $\phi_r^k \in [0, \pi]$ and $\psi_r^k \in [0, \pi]$ are the elevation and azimuth AoAs at the CU, respectively. The receive response vector for the fluid antenna at the CU is then given by

$$\mathbf{f}(\mathbf{r}) \triangleq \left[e^{j\frac{2\pi}{\lambda}\rho_r^1(\mathbf{r})}, \ldots, e^{j\frac{2\pi}{\lambda}\rho_r^{p_r}(\mathbf{r})} \right]^T \in \mathbb{C}^{p_r \times 1}, \tag{6}$$

where p_r represents the number of receive paths.

Furthermore, we define the path response matrix from $\mathbf{t}_0$ to $\mathbf{r}_0$ as $\boldsymbol{\Sigma} \in \mathbb{C}^{p_r \times p_t}$, where $\Sigma_{i,k}$ represents the response between

---

the i-th transmit path and the k-th receive path. Hence, the channel vector from the BS to the CU can be expressed by

$$\mathbf{h}(\overline{\mathbf{t}}, \mathbf{r}) = \mathbf{f}^H(\mathbf{r})\boldsymbol{\Sigma}\mathbf{E}(\overline{\mathbf{t}}). \tag{7}$$

In the proposed ISAC system, the BS transmits the signals to the CU to achieve the communication function. Hence, the communication rate is considered as the performance metric, which is given by

$$R = \log_2 \left(1 + \frac{\mathbf{h}(\overline{\mathbf{t}}, \mathbf{r})\mathbf{V}\mathbf{h}^H(\overline{\mathbf{t}}, \mathbf{r})}{\sigma_w^2} \right), \tag{8}$$

where $\mathbf{V} = \mathbf{v}\mathbf{v}^H$.

Parallel to this, the BS also employs the beamforming technique to enhance the sensing function. This approach is designed to direct a strong beampattern toward potential targets, thereby increasing the radar signal-to-noise ratio (SNR) and ultimately improving sensing performance [19], [20]. Consequently, the sensing beampattern gain is adopted as the metric for sensing performance, which is quantified by

$$\mathbf{p}(\overline{\mathbf{t}}) = \mathrm{Tr}\left(\mathbf{E}(\overline{\mathbf{t}})\mathbf{V}\mathbf{E}^H(\overline{\mathbf{t}}) \right). \tag{9}$$

C. Problem Formulation

We aim to maximize the communication rate while adhering to the constraints on the transmit power of the BS and the sensing beampattern gain. The optimizing variables include the transmit beamforming matrix $\mathbf{V}$, the locations of the transmit fluid antennas $\overline{\mathbf{t}}$, and the location of the receive fluid antenna $\mathbf{r}$. Thus, the optimization problem can be formulated as

$$\max_{\overline{\mathbf{t}}, \mathbf{r}, \mathbf{V} \succeq \mathbf{0}} \quad R \tag{10a}$$

$$\text{s.t.} \quad \overline{\mathbf{t}} \in \mathcal{S}_t, \tag{10b}$$

$$\mathbf{r} \in \mathcal{S}_r, \tag{10c}$$

$$||\mathbf{t}_n - \mathbf{t}_v||_2 \geq D, \ n, v \in \mathcal{N}, \ n \neq v, \tag{10d}$$

$$\mathrm{Tr}(\mathbf{V}) \leq P_{\max}, \tag{10e}$$

$$\mathrm{Tr}\left(\mathbf{E}(\overline{\mathbf{t}})\mathbf{V}\mathbf{E}^H(\overline{\mathbf{t}}) \right) \geq \Gamma, \tag{10f}$$

where (10d) is the minimum distance requirement between the antennas in the transmit region to avoid coupling; (10e) denotes the maximum transmit power constraint of the BS; (10f) represents the sensing beampattern gain requirement.

However, due to the highly non-convex objective function (10a), constraints (10d) and (10f), solving (10) becomes exceedingly challenging. To address this issue, we employ an AO algorithm, whose details are given in the following section.

III. AO Algorithm

Here, adhering to the procedure of the AO algorithm, we decompose (10) into three sub-problems and convert them into convex forms. Subsequently, we alternately optimize these sub-problems, obtaining a locally optimal solution for (10).

---

[1] We are abusing the word 'move' here to mean the relocation of an antenna. In practice, this may be achieved by changing the location of the antenna aperture by using reconfigurable pixel technologies, which does not involve physical movement of any radiating structure.

A. Optimization of Transmit Covariance Matrix

When the locations $\bar{\mathbf{t}}$ and $\mathbf{r}$ are fixed, Problem (10) is reformulated as

$$\max_{\mathbf{V} \succeq \mathbf{0}} \quad R \tag{11a}$$

$$\text{s.t.} \quad \text{Tr}(\mathbf{V}) \leq P_{\max}, \tag{11b}$$

$$\text{Tr}\left(\mathbf{E}(\bar{\mathbf{t}})\mathbf{V}\mathbf{E}^H(\bar{\mathbf{t}})\right) \geq \Gamma. \tag{11c}$$

Given that the objective function is concave with respect to $\mathbf{V}$ and the constraints (11b) and (11c) are linear with respect to $\mathbf{V}$, (11) is inherently convex. Thus, it can be efficiently solved using the convex programming toolbox CVX [21].

B. Optimization of Transmit Fluid Antenna Location

In this subsection, we focus on optimizing the locations of the transmit fluid antennas $\bar{\mathbf{t}}$, given fixed conditions for $\mathbf{V}$ and $\mathbf{r}$. Since $\log_2(1+x)$ is an increasing function with respect to x, maximizing the communication rate R in Problem (10) is equivalent to maximizing the power term $\mathbf{h}(\bar{\mathbf{t}},\mathbf{r})\mathbf{V}\mathbf{h}^H(\bar{\mathbf{t}},\mathbf{r})$. Noting that this term is a scalar, we can reformulate the optimization problem as

$$\max_{\bar{\mathbf{t}}} \quad \text{Tr}\left(\mathbf{h}(\bar{\mathbf{t}},\mathbf{r})\mathbf{V}\mathbf{h}^H(\bar{\mathbf{t}},\mathbf{r})\right) \tag{12a}$$

$$\text{s.t.} \quad (10b), (10d), (10f). \tag{12b}$$

Utilizing the properties of the matrix trace, the objective function in Problem (12) can be equivalently rewritten as

$$\text{Tr}\left(\mathbf{h}^H(\bar{\mathbf{t}},\mathbf{r})\mathbf{h}(\bar{\mathbf{t}},\mathbf{r})\mathbf{V}\right) = \text{Tr}\left(\sum_{n=1}^{N} s(\mathbf{t}_n)s^H(\mathbf{t}_n)\mathbf{V}\right), \tag{13}$$

where $s(\mathbf{t}_n) = \mathbf{f}^H(\mathbf{r})\boldsymbol{\Sigma}\mathbf{e}(\mathbf{t}_n) \in \mathbb{C}^{1 \times 1}$. Assuming $\{\mathbf{t}_j, j \neq n\}_{j=1}^{N}$ are fixed, maximizing (13) is equivalent to maximizing

$$\text{Tr}\left(s(\mathbf{t}_n)s^H(\mathbf{t}_n)\right) = s^H(\mathbf{t}_n)s(\mathbf{t}_n)$$
$$= \underbrace{\mathbf{e}^H(\mathbf{t}_n)\mathbf{A}_n\mathbf{e}(\mathbf{t}_n)}_{g(\mathbf{t}_n)}, \tag{14}$$

where $\mathbf{A}_n = \boldsymbol{\Sigma}^H\mathbf{f}(r)\mathbf{f}^H(r)\boldsymbol{\Sigma} \in \mathbb{C}^{p_t \times p_t}$ is independent of $\mathbf{t}_n$. Recognizing that $g(\mathbf{t}_n)$ is convex with respect to $\mathbf{e}(\mathbf{t}_n)$, we approximate $g(\mathbf{t}_n)$ using its first-order Taylor expansion around the point $\hat{\mathbf{t}}_n$ as a lower bound for the objective function:

$$g(\mathbf{t}_n; \hat{\mathbf{t}}_n) = \underbrace{2\,\Re\left\{\mathbf{e}^H(\hat{\mathbf{t}}_n)\mathbf{A}_n\mathbf{e}(\mathbf{t}_n)\right\}}_{\widehat{g}(\mathbf{t}_n)} - \underbrace{\mathbf{e}^H(\hat{\mathbf{t}}_n)\mathbf{A}_n\mathbf{e}(\hat{\mathbf{t}}_n)}_{\text{constant}}. \tag{15}$$

Thus, maximizing $g(\mathbf{t}_n)$ can be simplified to maximize $\widehat{g}(\mathbf{t}_n)$.

Addressing non-convex constraints, for (10d), we observe that $\|\mathbf{t}_n - \mathbf{t}_v\|_2$ is convex with respect to $\mathbf{t}_n$. Employing the first-order Taylor expansion of $\|\mathbf{t}_n - \mathbf{t}_v\|_2$ around $\hat{\mathbf{t}}_n$ provides a lower bound, which is given by

$$f(\mathbf{t}_n; \hat{\mathbf{t}}_n) = \frac{1}{\|\hat{\mathbf{t}}_n - \mathbf{t}_v\|_2}(\hat{\mathbf{t}}_n - \mathbf{t}_v)^T(\mathbf{t}_n - \mathbf{t}_v). \tag{16}$$

For constraint (10f), defining the n-th element of $\mathbf{v}$ as $v(n) \in \mathbb{C}^{1 \times 1}$, (10f) can be reformulated as

$$\text{Tr}\left(\mathbf{E}(\bar{\mathbf{t}})\mathbf{V}\mathbf{E}^H(\bar{\mathbf{t}})\right) = \widetilde{g}(\mathbf{t}_n) + 2\Re\left\{\mathbf{e}^H(\mathbf{t}_n)\boldsymbol{\kappa}\right\} + d_1, \tag{17}$$

with the detailed proof of (17) shown at the top of next page.

It can be observed that $\widetilde{g}(\mathbf{t}_n)$ is convex with respect to $\mathbf{e}(\mathbf{t}_n)$. To exploit this, we apply a first-order Taylor expansion around a point $\hat{\mathbf{t}}_n$ to serve as a lower bound for the following objective function:

$$\widetilde{g}(\mathbf{t}_n; \hat{\mathbf{t}}_n) = 2\Re\left\{v(n)v^H(n)\mathbf{e}^H(\mathbf{t}_n)\mathbf{e}(\hat{\mathbf{t}}_n)\right\} - \underbrace{v(n)v^H(n)\mathbf{e}^H(\hat{\mathbf{t}}_n)\mathbf{e}(\hat{\mathbf{t}}_n)}_{d_2}. \tag{19}$$

By using (19), we can rewrite constraint (10f) as

$$\text{Tr}\left(\mathbf{E}(\bar{\mathbf{t}})\mathbf{V}\mathbf{E}^H(\bar{\mathbf{t}})\right) = \underbrace{2\Re\left\{\mathbf{e}^H(\mathbf{t}_n)\boldsymbol{\eta}\right\}}_{\overline{g}(\mathbf{t}_n)} + d_1 - d_2, \tag{20}$$

where $\boldsymbol{\eta} = v(n)v^H(n)\mathbf{e}(\hat{\mathbf{t}}_n) + \boldsymbol{\kappa}$. Subsequent analysis reveals that $\overline{g}(\mathbf{t}_n)$ and $\widehat{g}(\mathbf{t}_n)$, functions related to $\mathbf{t}_n$, are neither concave nor convex. Thus, the first-order Taylor expansion is inadequate for these functions. Alternatively, we propose a surrogate function by employing the second-order Taylor expansion to obtain the lower bounds of them [11], [12]. Specifically, we have

$$\widehat{g}(\mathbf{t}_n; \hat{\mathbf{t}}_n) = \widehat{g}(\hat{\mathbf{t}}_n) + \nabla\widehat{g}(\hat{\mathbf{t}}_n)^T(\mathbf{t}_n - \hat{\mathbf{t}}_n) - \frac{\widehat{\delta}_n}{2}(\mathbf{t}_n - \hat{\mathbf{t}}_n)^T(\mathbf{t}_n - \hat{\mathbf{t}}_n), \tag{21}$$

$$\overline{g}(\mathbf{t}_n; \hat{\mathbf{t}}_n) = \overline{g}(\hat{\mathbf{t}}_n) + \nabla\overline{g}(\hat{\mathbf{t}}_n)^T(\mathbf{t}_n - \hat{\mathbf{t}}_n) - \frac{\overline{\delta}_n}{2}(\mathbf{t}_n - \hat{\mathbf{t}}_n)^T(\mathbf{t}_n - \hat{\mathbf{t}}_n), \tag{22}$$

where $\nabla\overline{g}(\mathbf{t}_n)$ and $\nabla^2\overline{g}(\mathbf{t}_n)$ are the gradient and Hessian matrix of $\overline{g}(\mathbf{t}_n)$, respectively, and similarly for $\widehat{g}(\mathbf{t}_n)$. We introduce scalars $\overline{\delta}_n$ and $\widehat{\delta}_n$ such that $\overline{\delta}_n\mathbf{I}_2 \succeq \nabla^2\overline{g}(\mathbf{t}_n)$ and $\widehat{\delta}_n\mathbf{I}_2 \succeq \nabla^2\widehat{g}(\mathbf{t}_n)$, as derived in [11, Appendix B]. This formulation leads to the following convex optimization problem:

$$\max_{\mathbf{t}_n} \quad \widehat{g}(\mathbf{t}_n; \mathbf{t}_n^{(m)}) \tag{23a}$$

$$\text{s.t.} \quad \bar{\mathbf{t}} \in \mathbf{S}_t, \tag{23b}$$

$$f(\mathbf{t}_n; \mathbf{t}_n^{(m)}) \geq D, u, n \in \mathcal{N}, \; u \neq n, \tag{23c}$$

$$\overline{g}(\mathbf{t}_n; \mathbf{t}_n^{(m)}) \geq \frac{\Gamma + d_2 - d_1}{2}, \tag{23d}$$

where $\mathbf{t}_n^{(m)}$ is the optimal $\mathbf{t}_n$ of the m-th iteration.

The objective functions in (23a) is characterized as concave with respect to $\mathbf{t}_n$. Moreover, the constraints (23b) and (23c) are linear with respect to $\mathbf{t}_n$. Consequently, the optimization problem defined in (23) is convex, facilitating its resolution via established convex optimization methods [21].

C. Optimization of Receive Fluid Antenna Location

In this subsection, our objective is to optimize the location $\mathbf{r}$ of receive fluid antenna with given $\mathbf{V}$ and $\bar{\mathbf{t}}$, and the optimization problem is given by

$$\max_{\mathbf{r}} \quad \text{Tr}\left(\mathbf{h}(\bar{\mathbf{t}},\mathbf{r})\mathbf{V}\mathbf{h}^H(\bar{\mathbf{t}},\mathbf{r})\right) \tag{24a}$$

$$\text{s.t.} \quad (10c). \tag{24b}$$

$$\text{Tr}\left(\mathbf{E}(\bar{\mathbf{t}})\mathbf{v}\mathbf{v}^H\mathbf{E}(\bar{\mathbf{t}})^H\right) = \text{Tr}\left(\left[\sum_{n=1}^{N}\mathbf{e}(\mathbf{t}_n)v(n)\right]\left[\sum_{n=1}^{N}v^H(n)\mathbf{e}^H(\mathbf{t}_n)\right]\right)$$

$$= \text{Tr}\left(\underbrace{v(n)v^H(n)\mathbf{e}^H(\mathbf{t}_n)\mathbf{e}(\mathbf{t}_n)}_{\widetilde{g}(\mathbf{t}_n)}\right) + \text{Tr}\left(\mathbf{e}(\mathbf{t}_n)v(n)\sum_{i\neq n}^{N}v^H(i)\mathbf{e}^H(\mathbf{t}_i)\right)$$

$$+ \text{Tr}\left(\underbrace{\sum_{j\neq n}^{N}\mathbf{e}(\mathbf{t}_j)v(j)v^H(n)\,\mathbf{e}^H(\mathbf{t}_n)}_{\kappa}\right) + \underbrace{\text{Tr}\left(\sum_{j\neq n}^{N}\mathbf{e}(\mathbf{t}_j)v(j)\sum_{i\neq n}^{N}v^H(i)\mathbf{e}^H(\mathbf{t}_i)\right)}_{d_1} \quad (18)$$

Consider the eigenvalue decomposition (EVD) of the matrix $\mathbf{V}$, denoted by $\mathbf{V} = \mathbf{U}_V\boldsymbol{\Lambda}_V\mathbf{U}_V^H$, where $\mathbf{U}_V \in \mathbb{C}^{N\times N}$ consists of the eigenvectors and $\boldsymbol{\Lambda}_V \in \mathbb{C}^{N\times N}$ is a diagonal matrix containing the eigenvalues. Then we define $\mathbf{Z}(\mathbf{r}) = \mathbf{h}(\bar{\mathbf{t}}, \mathbf{r})\mathbf{U}_V\boldsymbol{\Lambda}_V^{\frac{1}{2}} \in \mathbb{C}^{1\times N}$ and $\mathbf{z}(\mathbf{r}) = \boldsymbol{\Lambda}_V^{\frac{1}{2}}\mathbf{U}_V^H\mathbf{E}^H(\bar{\mathbf{t}})\boldsymbol{\Sigma}^H\mathbf{f}(\mathbf{r}) \in \mathbb{C}^{N\times 1}$. Thus, the objective function (24a) can be written as

$$\text{Tr}\left(\mathbf{h}(\bar{\mathbf{t}}, \mathbf{r})\mathbf{V}\mathbf{h}^H(\bar{\mathbf{t}}, \mathbf{r})\right) = \text{Tr}\left(\mathbf{Z}(\mathbf{r})\mathbf{Z}^H(\mathbf{r})\right)$$
$$= \mathbf{z}^H(\mathbf{r})\mathbf{z}(\mathbf{r})$$
$$= \mathbf{f}^H(\mathbf{r})\mathbf{B}_m\mathbf{f}(\mathbf{r}), \quad (25)$$

where $\mathbf{B}_m = \boldsymbol{\Sigma}\mathbf{E}(\bar{\mathbf{t}})\mathbf{U}_V\boldsymbol{\Lambda}_V^{\frac{1}{2}}\boldsymbol{\Lambda}_V^{\frac{1}{2}}\mathbf{U}_V^H\mathbf{E}^H(\bar{\mathbf{t}})\boldsymbol{\Sigma}^H$. Thus, Problem (24) is rewritten as

$$\max_{\mathbf{r}} \quad \mathbf{f}^H(\mathbf{r})\mathbf{B}_m\mathbf{f}(\mathbf{r}_m) \quad (26a)$$
$$\text{s.t.} \quad (10c). \quad (26b)$$

Similar to the optimization of transmit fluid antenna locations, we also use the second-order Taylor expansion to transform the objective function into a concave quadratic function. Then, Problem (24) can be transformed as convex form [22].

The aforementioned procedures for solving Problem (10) is summarized in Algorithm 1, where the optimal $\bar{\mathbf{t}}$, $\mathbf{r}$, and $\mathbf{V}$ in the lth iteration are denoted as $\bar{\mathbf{t}}^{(l)}$, $\mathbf{r}^{(l)}$, and $\mathbf{V}^{(l)}$, respectively.

Algorithm 1 The Proposed Alternating Optimization Algorithm

1: **Initialize:** $l = 0$, $\mathbf{V}^{(0)}$, $\bar{\mathbf{t}}^{(0)}$, and $\mathbf{r}^{(0)}$;
2: **Repeat**
    $l := l + 1$;
    Update $\mathbf{V}^{(l)}$ by (11);
    Update $\bar{\mathbf{t}}^{(l)}$ by (23);
    Update $\mathbf{r}^{(l)}$ by (26);
3: **Until:** Convergence.

IV. NUMERICAL RESULTS

In our simulation experiments, we consider that the elevation and azimuth angles $\phi_t^i, \psi_t^i, \phi_r^k, \psi_r^k$ are all independent and identically distributed variables randomly distributed in $[0, \pi]$. The convergence accuracy is set to 10^{-3}. The minimum distance constraint between the fluid antennas is set to $D = \lambda/2$

and restricted to movement within the range of $A \times A$. The path response matrix is assumed to be diagonal with $\boldsymbol{\Sigma}[1,1] \sim \mathcal{CN}(0, \tau/(\tau+1))$ and $\boldsymbol{\Sigma}[k,k] \sim \mathcal{CN}(0, 1/(\tau+1)(p_r-1))$ for $k = 2, 3, \ldots, p_r$, where $\tau = 1$ represents the ratio of the average power of the line-of-sight (LoS) path to the average power of the non-line-of-sight (NLoS) path. We assume that the number of transmit and receive paths as $p_t = p_r = 3$, the maximum transmit SNR of the BS is $P_{\max}/\sigma_w^2 = 5$ dB, and the ratio of the minimum sensing beampattern gain and noise power is $\Gamma/\sigma_w^2 = 9$ dB. We also set $N = 4$ and $A = 4\lambda$.

In Fig. 1, we demonstrate the convergence behavior of our proposed alternating optimization algorithm, where $N = 2$, 3, and 4. From Fig. 1, it is observed that our proposed alternating optimization algorithm converges after about 9 iterations. Besides, we can also find that the communication rate increases with the increasing of N.

In Fig. 2, we study the communication rate versus the maximum transmit SNR of the BS $P_{\max}/\sigma_w^2$. In the legend, "Proposed" denotes our proposed AO algorithm based scheme, while "RFA" means the scheme that the BS is equipped with an N-element uniform linear array spaced by $\lambda/2$, and the CU is equipped with a single fluid antenna. "FPA" represents the scheme that the BS and CU are both equipped with FPAs. We can observe from the results in Fig. 2 that the larger $P_{\max}/\sigma_w^2$, the larger the communication rate. Moreover, at the same SNR, the "Proposed" scheme consistently achieves higher rates compared to the other schemes.

Fig. 3 illustrates the impact of normalized fluid antenna mobility regions A/λ on the communication rate. It can be observed that the communication rates of all schemes except for "FPA" scheme increase as A/λ increases. This is because the location of antennas of the "FPA" scheme is fixed, and the enhancement of A/λ cannot improve the communication performance of the "FPA" scheme. Moreover, we can find that the "Proposed" scheme and the "RFA" scheme exhibit the significant enhancement in communication rates compared with the "FPA" scheme. This is attributed to the larger mobility region can provide larger DoFs. Moreover, we can also find that the lines of the "Proposed" scheme and the "RFA" scheme become constant, when A/λ is larger than 4. This indicates that the considered system can achieve the maximum communication rate within a finite movable region.

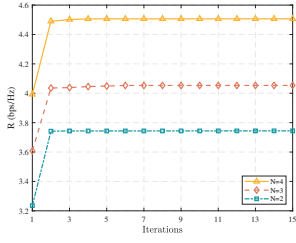Fig. 4 compares the impact of the ratio of the minimum

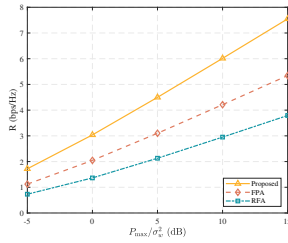Fig. 1. Convergence of the proposed algorithm.

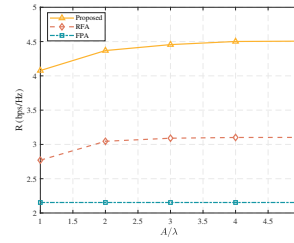Fig. 2. $P_{\max}/\sigma_w^2$ versus communication rate.

Fig. 3. A/λ versus communication rate.
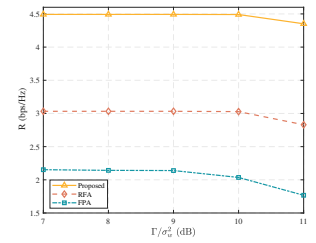
Fig. 4. Γ/σ_w^2 versus communication rate.

sensing beampattern gain and noise power Γ/σ_w^2 on the communication rate. It can be observed from Fig. 4 that the achievable communication rates of all schemes decrease as Γ/σ_w^2 increases. This is because the BS needs to utilize more spatial resource to ensure sensing performance, thereby impairing the communication performance. Besides, the "Proposed" scheme can effectively overcome the impact of sensing performance requirement by optimizing the fluid antenna locations, and achieves the largest communication rate.

V. Conclusion

In this letter, we investigated a fluid antenna-assisted ISAC system, and maximized the communication rate between the BS and the CU with the requirements of the transmit power of the BS and the sensing beampattern gain. Due to the highly non-convex nature of the problem, we utilized an AO algorithm to obtain a locally optimal solution. Numerical results demonstrated that our proposed scheme outperforms traditional schemes in term of communication performance under the same sensing performance constraint. Furthermore, with increasing of the fluid antenna area, our proposed scheme achieves a higher communication rate.

References

[1] W. Saad, M. Bennis, and M. Chen, "A vision of 6G wireless systems: Applications, trends, technologies, and open research problems," *IEEE Netw.*, vol. 34, no. 3, pp. 134–142, May 2020.

[2] F. Liu *et al.*, "Joint radar and communication design: Applications, state-of-the-art, and the road ahead," *IEEE Trans. Commun.*, vol. 68, no. 6, pp. 3834–3862, Jun. 2020.

[3] S. Lu *et al.*, "Integrated sensing and communications: Recent advances and ten open challenges," *IEEE Internet Things J.*, vol. 11, no. 11, pp. 19094–19120, Jun. 2024.

[4] J. Yao, L. Mai, and Q. Zhang, "Approximate capacity-distortion region of joint state sensing and communication in MIMO real Gaussian channels," *IEEE Trans. Commun.*, vol. 72, no. 5, pp. 2625–2638, May 2024.

[5] Y. Zhou *et al.*, "Secure communications for UAV-enabled mobile edge computing systems," *IEEE Trans. Commun.*, vol. 68, no. 1, pp. 376–388, Jan. 2020.

[6] Y. Chen, H. Hua, J. Xu, and D. W. K. Ng, "ISAC meets SWIPT: Multi-functional wireless systems integrating sensing, communication, and powering," *IEEE Trans. Wireless Commun.*, early access, doi: 10.1109/TWC.2023.3338626, 2024.

[7] Z. Cui, J. Hu, J. Cheng, and G. Li, "Multi-domain NOMA for ISAC: Utilizing the DOF in the delay-doppler domain," *IEEE Commun. Lett.*, vol. 27, no. 2, pp. 726–730, Feb. 2023.

[8] N. Su, F. Liu, and C. Masouros, "Sensing-assisted eavesdropper estimation: An ISAC breakthrough in physical layer security," *IEEE Trans. Wireless Commun.*, vol. 23, no. 4, pp. 3162–3174, Apr. 2024.

[9] K. K. Wong, A. Shojaeifard, K.-F. Tong, and Y. Zhang, "Performance limits of fluid antenna systems," *IEEE Commun. Lett.*, vol. 24, no. 11, pp. 2469–2472, Nov. 2020.

[10] K.-K. Wong, A. Shojaeifard, K.-F. Tong, and Y. Zhang, "Fluid antenna systems," *IEEE Trans. Wireless Commun.*, vol. 20, no. 3, pp. 1950–1962, Mar. 2021.

[11] W. Ma, L. Zhu, and R. Zhang, "MIMO capacity characterization for movable antenna systems," *IEEE Trans. Wireless Commun.*, vol. 23, no. 4, pp. 3392–3407, Apr. 2023.

[12] L. Zhu, W. Ma, B. Ning, and R. Zhang, "Movable-antenna enhanced multiuser communication via antenna position optimization," *IEEE Trans. Wireless Commun.*, early access, doi:10.1109/TWC.2023.3338626, 2023.

[13] L. Zhu and K. K. Wong, "Historical review of fluid antenna and movable antenna," *arXiv preprint*, arXiv:2401.02362v2, 2024.

[14] S. Yang, W. Lyu, B. Ning, Z. Zhang, and C. Yuen, "Flexible precoding for multi-user movable antenna communications," *IEEE Wireless Commun. Lett.*, vol. 13, no. 5, pp. 1404–1408, May 2024.

[15] J. Zheng *et al.*, "FAS-assisted NOMA short-packet communication systems," *IEEE Trans. Veh. Technol.*, early access, doi:10.1109/TVT.2024.3363115, 2024.

[16] G. Hu, Q. Wu, K. Xu, J. Si, and N. Al-Dhahir, "Secure wireless communication via movable-antenna array," *IEEE Signal Process. Lett.*, vol. 31, pp. 516–520, Jan. 2024.

[17] D. Zhang *et al.*, "Fluid antenna array enhanced over-the-air computation," *IEEE Wireless Commun. Lett.*, early access, doi:10.1109/LWC.2024.3378519, 2024.

[18] Y. Ye *et al.*, "Fluid antenna-assisted MIMO transmission exploiting statistical CSI," *IEEE Commun. Lett.*, vol. 28, no. 1, pp. 223–227, Jan. 2024.

[19] Z. He, W. Xu, H. Shen, Y. Huang, and H. Xiao, "Energy efficient beamforming optimization for integrated sensing and communication," *IEEE Wireless Commun. Lett.*, vol. 11, no. 7, pp. 1374–1378, Jul. 2022.

[20] Z. Liu *et al.*, "Joint transmit and receive beamforming design in full-duplex integrated sensing and communications," *IEEE J. Sel. Areas Commun.*, vol. 41, no. 9, pp. 2907–2919, Sept. 2023,

[21] M. Grant and S. Boyd, "CVX: MATLAB software for disciplined convex programming," [Online]. Available: http://cvxr.com/cvx.

[22] S. Boyd and L. Vandenberghe, *Convex Optimization*. Cambridge, U.K.: Cambridge Univ. Press, 2004